

RSC Advances



This is an *Accepted Manuscript*, which has been through the Royal Society of Chemistry peer review process and has been accepted for publication.

Accepted Manuscripts are published online shortly after acceptance, before technical editing, formatting and proof reading. Using this free service, authors can make their results available to the community, in citable form, before we publish the edited article. This *Accepted Manuscript* will be replaced by the edited, formatted and paginated article as soon as this is available.

You can find more information about *Accepted Manuscripts* in the [Information for Authors](#).

Please note that technical editing may introduce minor changes to the text and/or graphics, which may alter content. The journal's standard [Terms & Conditions](#) and the [Ethical guidelines](#) still apply. In no event shall the Royal Society of Chemistry be held responsible for any errors or omissions in this *Accepted Manuscript* or any consequences arising from the use of any information it contains.

Self-templating Noncatalyzed Synthesis of Monolithic Boron Nitride Nanowires

Chao-Hua Su^a, Ru-Zhi Wang*^a, Yue-Fei Zhang*^b, Xing-Wang Zhang^c, Hui Yan^a

^a College of Materials Science and Engineering, Beijing University of Technology, Beijing 100124, China

^b Institute of Microstructure and Properties of Advanced Materials, Beijing University of Technology, Beijing 100124, China

^c Key Laboratory of Semiconductor Materials Science, Institute of Semiconductors, Chinese Academy of Science, Beijing 100083, China

Abstract

Achieving economic orientation-controlled growth of monolithic nanowires remains a challenge. We report a simple and low-cost, endotaxial, self-templating, noncatalyzed synthesis of monolithic boron nitride semiconductor nanowires. The method uses orientated control of the nanowires prepared directly on Si substrates through plasma-enhanced chemical vapor deposition without catalyst. The growth direction of the synthetic monolithic nanowires is controlled as a function of substrate crystal orientation. We measured the vertical electrical properties of the nanowires. Our method provides an alternative strategy to control monolithic nanowire growth in substrates, and may allow for large-scale, low-cost nanowire device manufacture.

Keywords: boron nitride; monolithic nanowires; orientation control; catalyst-free

*To whom correspondence should be addressed. Email: wrz@bjut.edu.cn; yfzhang@bjut.edu.cn

Introduction

During the past decade, nanowires (NWs) have become an important subject of experimental and theoretical investigation in nanoscience and nanotechnology. They have been explored for use in a wide range of applications in electronics, photonics, and energy harvesting or conversion¹⁻³. Significant effort has been made to develop alternative methods to synthesize NWs with a desired chemical composition, diameter, and properties^{4, 5}. Control of the NW orientation and morphology is important in nanoscale device manufacture. Low-dimension boron nitride (BN) materials are a very promising inorganic nanosystem and have attracted great interest because of their excellent thermal and chemical stability and intrinsic electrical insulation^{6, 7}. Much interdependent research has focused on the synthesis of BN nanotubes, BN nanosheets and BN nanowires (BNNWs)⁸⁻¹⁰. However, challenges remain in fabricating single NW devices because it is difficult to produce monolithic BNNWs with tailored orientation.

Monolithic NW growth has been studied widely since monolithic NWs can be incorporated directly in devices and eliminate post-growth assembly in fabrication^{11, 12}. Template patterning allows for excellent control over placement and size, and this methodology is the most common approach to fabricate ordered arrays of NWs¹³⁻¹⁵. Lateral NW arrays can be prepared by fabricating grating templates or line structure materials followed by a transfer of the grating pattern to the substrate using an appropriate etching process¹⁶. Besides template patterning, strain-driven methods are also effective in the formation of monolithic NWs^{17, 18}. Zhang *et al.* reported that self-assembled Ge wires have been grown on Si(001) using a catalyst- and template-free method based on molecular beam epitaxy (MBE). Here the wires grow horizontally along either the [100] or the [010] direction¹⁸. Ge and Si have an excellent lattice match along the Si<100> orientation. The template patterning and strain-driven methods are not unique to the synthesis of monolithic NWs since the vapor–liquid–solid method can also be used¹⁹⁻²¹. However, the template patterning and MBE methods require complicated technology, and a significant cost factor has to be considered for lithography when using the MBE method. The common vapor–liquid–solid mechanism for NW production requires a metallic catalyst, which plays a critical role in NWs growth; however, it introduces metal contamination.

Increasing attention has been given to self-assembled endotaxial silicide NWs^{17, 22-26}. The term “endotaxy”, which was coined by Fathauer *et al.*²⁷, describes cases in which epitaxial growth occurs into the substrate¹⁷. Interesting and useful structures

can be formed by endotaxy, as in nanoscale permeable base transistors¹⁷ or thermoelectric devices^{28,29}. It is interesting that almost all reported endotaxial silicide NWs are extremely well aligned with a mutual orientation^{20, 23, 25}. Hence, in this research we wanted to determine whether it was feasible to use endotaxial silicide NWs as a template to synthesize monolithic NWs.

We synthesized monolithic BNNWs on Si substrates using plasma-enhanced chemical vapor deposition (PECVD) without any catalyst and template. The average BNNW length was ~ 10 μm , with a width of ~ 200 nm. The NW direction was controlled by the silicon substrate crystal orientation. For BNNW growth, N atoms permeate into the substrate to form endotaxial silicon nitride (Si_3N_4) and BNNW growth occurs on the endotaxial Si_3N_4 . This is a new self-templating and noncatalyzed synthesis method for BNNWs. This method avoids metal catalyst contamination and simplifies the template patterning process. This work may allow for the large-scale and low-cost fabrication of NW devices.

Materials and Methods

Sample preparation

BNNWs were prepared using an in-house PECVD system, which is shown schematically in Fig. 1. B_2O_3 powder (melting point $\sim 445^\circ\text{C}$) was used as a precursor. Radiofrequency (RF) power and a desired number of coils were used to ionize N_2 and H_2 as a substitute for ammonia (NH_3) gas. NH_3 has been used widely in the preparation of nitrides; however, since it is a toxic gas, an alternative source was used and substituted for by N_2 and H_2 . The B_2O_3 powders were placed into a quartz boat and transferred into the center of the tube furnace. Three different crystal-orientated Si substrates (Si(100), Si(110) and Si(111)) partly covered the quartz boat. Pure N_2 was used to purge the air in the tube furnace prior to initiating the experiments. The furnace was heated to 1000°C at $10^\circ\text{C}/\text{min}$ under N_2 and after reaching the operating temperature, the H_2 inlet was opened and the RF power was switched on. N_2 and H_2 flows were 20 sccm and 10 sccm, respectively, with a working internal pressure of ~ 45 Pa. The reaction was held under these conditions for 1 h. Thereafter the RF power and the H_2 flow were isolated and the furnace was cooled to $\sim 450^\circ\text{C}$ under N_2 followed by further cooling to room temperature. The experimental process is simple, nontoxic, and low-cost and can be used for large-scale preparation.

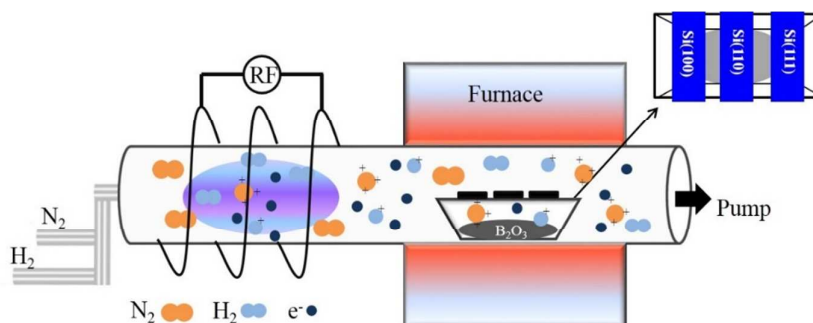


Fig. 1 Schematic of PECVD system.

Characterization

The morphology of as-synthesized NWs was studied by scanning electron microscopy (SEM; Hitachi S4800) and atomic force microscopy (AFM; Solver P47). To understand the microstructures of the obtained NWs and their interfacial relationship with the silicon substrate, focus ion beam (FIB) microscopy (FEI Helios Nanolab 600i) was applied to localized sites of interest to prepare transmission electron microscopy (TEM, TecnaiG2 F30) samples. For axial direction TEM samples, we randomly selected one NW and used FIB to thin the NW in the axial direction. For cross-sectional samples, we randomly selected two parallel NWs on Si(100) and used FIB to thin the NWs in the radial direction. The chemical composition of the NW was analyzed by electron energy loss spectroscopy (EELS) in a JEOL 2010F and the vertical electrical properties of the NWs were measured by conductive AFM (C-AFM) in a Bruker Dimension Icon.

Results and Discussion

Orientation of monolithic NWs

Figure 2a–c show SEM micrographs of as-synthesized monolithic NWs on varying crystallographic Si substrates. The average NW length was ~ 10 μm , with a maximum length of 30–40 μm . A correlation exists between Si substrate orientation and NW growth direction. The NW growth directions on the Si(100) substrate are mutually orthogonal and are limited in two directions. A perfect right angle exists for two NWs as shown in Fig. 2g. For the Si(110) substrate, the NWs display growth in one crystallographic direction only. Whereas on the Si(111) substrate, growth occurs in three directions, each at 60° to each other, as shown in Fig. 2h. As illustrated in the schematics in Fig. 2d–f, NWs grow along the Si[011] and [0-11] crystallographic directions on the Si(100) substrate. With respect to the Si(110) substrate, the direction of growth is parallel to the [1-10] direction, and growth occurs in the Si[1-10], [-101], and [0-11] directions when the Si(111) substrate is used. From the angles between the

NWs and the primary flat surfaces of the Si wafers, the NW orientation is ascertained to be along equivalent Si $\langle 110 \rangle$ directions. Figure 3a–b show typical AFM images of NWs on Si(100). The height profile in Fig. 3c indicates that the NW height is ~ 20 nm and their width is ~ 180 nm. Figure 2h and b show that the individual NWs are nonconsecutive, but rather are a series of self-assembled quantum dots, which is also shown in the three-dimensional image of the NWs from the inset in Fig. 3a.

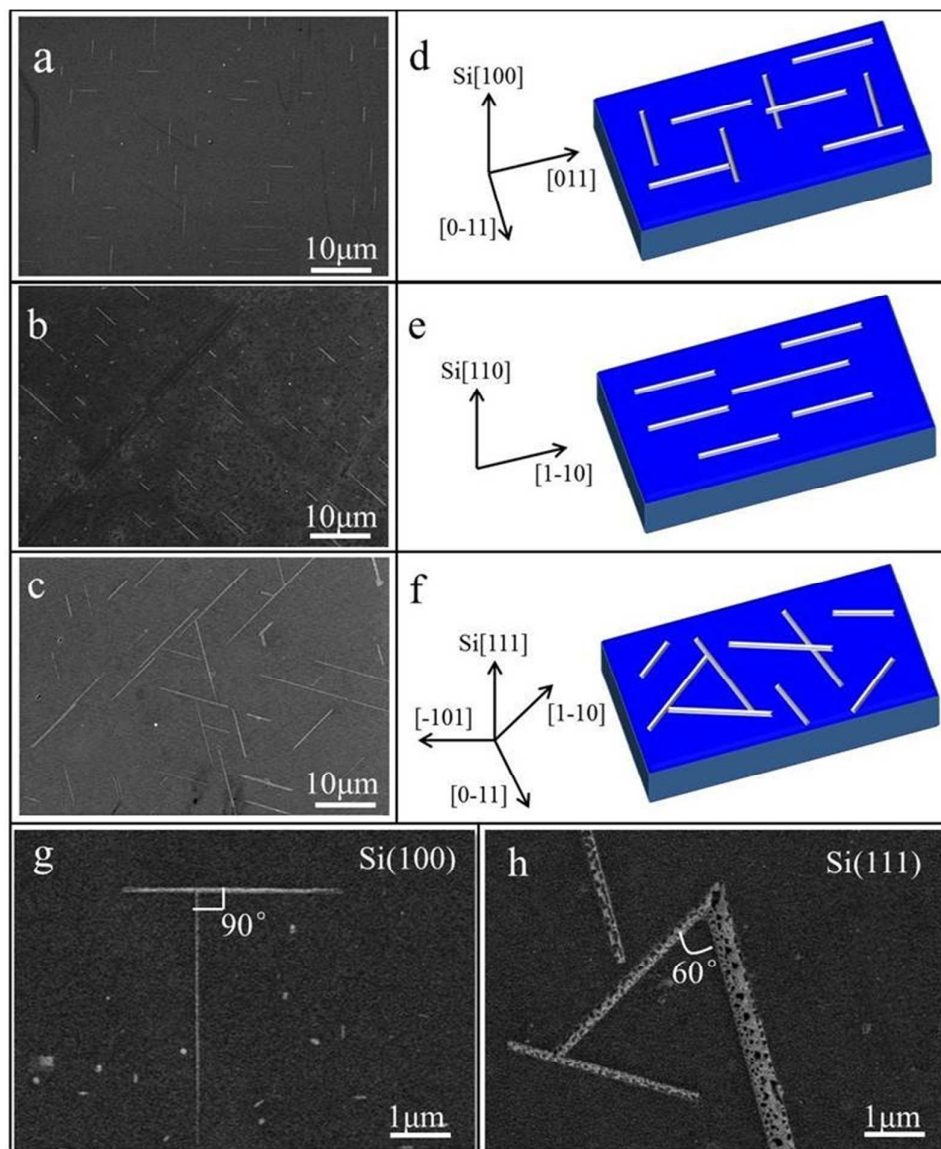


Fig. 2 (a–c) SEM micrographs of NWs grown on Si(110), (100), and (111) substrates, respectively. (d–f) Corresponding schematics illustrating NW growth directions. (g) Nanowires grown on Si(100) substrate showing a perfect right angle. (h) NWs grown on Si(111) substrate showing an equilateral triangle.

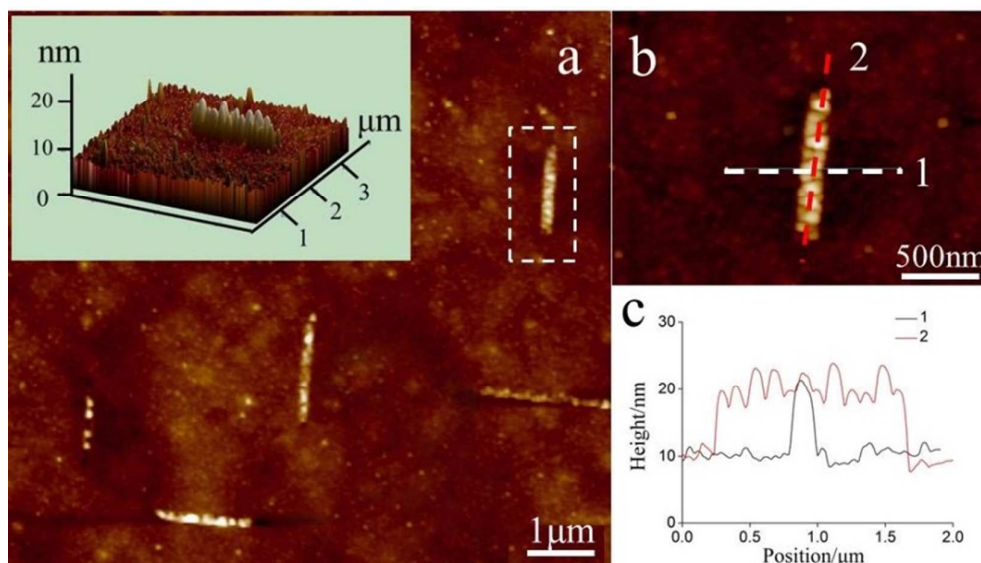


Fig. 3 (a, b) Typical AFM image of NWs grown on a Si(100) substrate. (c) Height profile along the line in (b).

Nanowire structures and composition on Si substrate

To clarify the NW structure and composition, TEM was used to analyze the microstructure of the NW growth at the interface. Figure 4a shows a TEM micrograph of the axial direction of the NW grown on Si(100). Three layers exist in the NW film with layer 3 being the Si substrate. Figure 5a and b (cross-sectional TEM micrographs of NWs) together show that the intermediate layer (layer 2) has grown into the substrate and is therefore deemed endotaxial²⁷. Layer 1 is composed of a series of amorphous nanodots that extend by growth into layer 2. Figure 4b shows the EELS spectrum that corresponds to the area of the endotaxial amorphous nanodots that are represented by a white rectangle in Fig. 4a. The B and N characteristic K-edges are visible in the EELS spectrum. Two distinct edges at 200 eV and 400 eV correspond to the B-K and N-K edges, respectively. Layer 1 is likely to be amorphous BN and many crystalline BN grains are contained within the amorphous BNNW, as shown in Fig. S1 (Supplementary information). Figure 4c shows an enlargement of the area inside the white rectangle in Fig. 4a. Two clear boundaries are visible: amorphous nanodot or endotaxial and endotaxial or Si substrate. A high-resolution TEM (HRTEM) micrograph (Fig. 4d) shows the interface between layer 2 and the Si substrate. A twin boundary exists at the interface, as denoted by the kinked white lines. The endotaxial interplanar spacing is ~ 0.27 nm, which is speculated to be silicide and not BN from the lattice parameters. The interplanar spacing is ~ 0.31 nm in the Si substrate, which corresponds to the Si(111) plane.

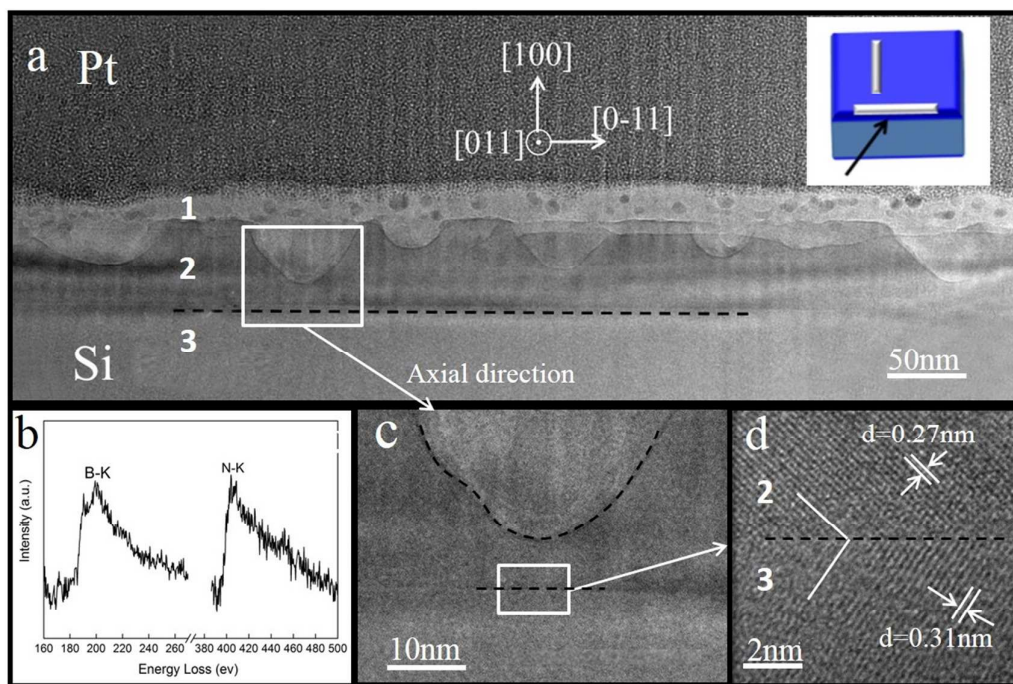


Fig. 4 (a) TEM micrograph of BNNW in the axial direction. (b) EELS spectrum corresponding to the area of amorphous nanodots from the white rectangle in Fig. 4a. (c) Enlarged area of white rectangle in Fig. 4a. (d) HRTEM micrograph of interface between intermediate layer 2 and Si substrate (layer 3).

For the cross-sectional microstructure study, we selected two random parallel NWs grown on Si(100), as shown in Fig. 5d, and used FIB to thin the NWs radially. Figure 5a and b show cross-sectional TEM micrographs of these two parallel NWs. The NWs have grown into the substrate. It is also evident that three types of structures exist: a top amorphous BN (layer 1), an endotaxial silicide (layer 2), and a Si substrate (layer 3). Figure 5c and e show lattice parameters from HRTEM analysis of the endotaxial silicide, which reveal that the endotaxy structure is Si_3N_4 (PDF#51-1334) and amorphous BNNWs grew on the endotaxial Si_3N_4 . Inset are the selected area electron diffraction patterns of the endotaxial Si_3N_4 in the radial direction. A periodical dislocation present at the interface of $\text{Si}_3\text{N}_4/\text{Si}$ is visible in Fig. 5a and b, as indicated by the white circle. The NW/substrate interface between the two NWs varies. In Fig. 5a, the interfacial angle (the angle between each plane of the Si(111) crystallographic form and the Si(001) plane) between the Si(001) surface and the NW is $\sim 55^\circ$. This suggests that the N atom prefers to diffuse stepwise in the Si<111> direction. Previous reports have concluded that the Si(111) plane is highly likely to form an interface with NWs^{17, 20, 23, 24, 26}. However, in Fig. 5b, the interfacial angle between the Si(001) surface and the NW is $\sim 63^\circ$, which is parallel to crystallographic

planes of the Si(102) form. This would suggest that the N atom would prefer to diffuse in the Si<102> direction. To the best of our knowledge, this is the first reporting of such findings.

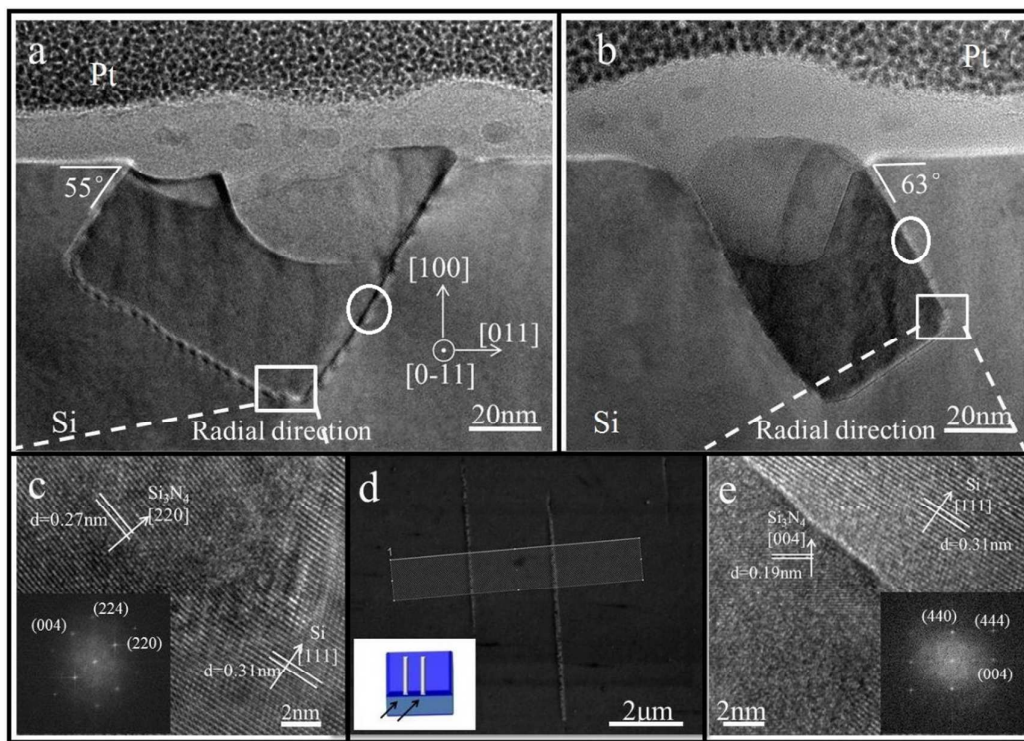


Fig. 5 (a, b) Cross-sectional TEM micrographs of two parallel BNNWs. (c, e) HRTEM micrographs of interface between endotaxial Si₃N₄ and silicon substrate. The Si₃N₄ region shows a darker contrast, and a coherent interface was formed between Si₃N₄/Si. Insets are the respective selected area electron diffraction patterns of the NW in the radial direction. (d) SEM micrograph of two parallel NWs.

Two-step growth induced by mixed interface

Previous reports on endotaxial NW growth were by anisotropic crystal growth into the substrate from the interdiffusion of formation elements, breaking of crystal surface symmetry, and NW growth in the substrate^{20, 23}. To the best of our knowledge, no related reports exist on compound semiconductor NW growth on endotaxial NWs. We used an endotaxial NW self-template to synthesize BNNWs. Endotaxial silicide NWs were formed first, followed by endotaxial silicide that served as a template to synthesize outer layer NWs. Figures 3a and 4a and b show that an amorphous BN layer grew on the Si₃N₄ and that the BN nanodots permeated into the Si₃N₄. BN thin film epitaxial growth exists on the substrate. As shown in Fig. S2, NWs grow only exactly above endotaxial Si₃N₄. Therefore, it is obvious that endotaxial Si₃N₄ NWs are

intrinsic self-templates for monolithic BN NW growth.

A possible explanation for the orientation-control growth of monolithic BNNWs is as follows. High RF power ionizes the H₂ and N₂ molecules into active atoms or ions with high energy. Later B₂O₃ reacts with H and N and results in BN film deposition on the Si substrate. Besides BN synthesis, the surface structure of the Si substrate is destroyed by high energy N or H atoms or ions and forms some defects along Si<110>. Many studies have shown that the Si<110> direction is very active and exhibits anisotropic diffusion in crystalline Si. Previous reports have shown that hydrogen and silicon atoms can diffuse with lower activation energies along Si <110>^{30, 31}, and the self-diffusion of Si atoms in bulk or on the Si surface also tends to follow <110> directions^{32, 33}. Several in-plane silicide NWs grown on Si substrates align along Si <110>^{17, 19, 20, 26, 34} regardless of the presence or absence of a catalyst. It is feasible that after N or H atom or ion bombardment of the Si surface, the Si<110> direction forms defects preferentially. Surfaces where the defects form are unstable compared with other areas, therefore N atoms or ions diffuse along a certain plane into the Si substrate and form endotaxial Si₃N₄ in defects. The BN vapor prefers to concentrate in defects. The probability of BN nucleation on endotaxial Si₃N₄ is higher than in other areas and this results in a series of BN nanodots, which then self-assemble into NWs as observed from SEM.

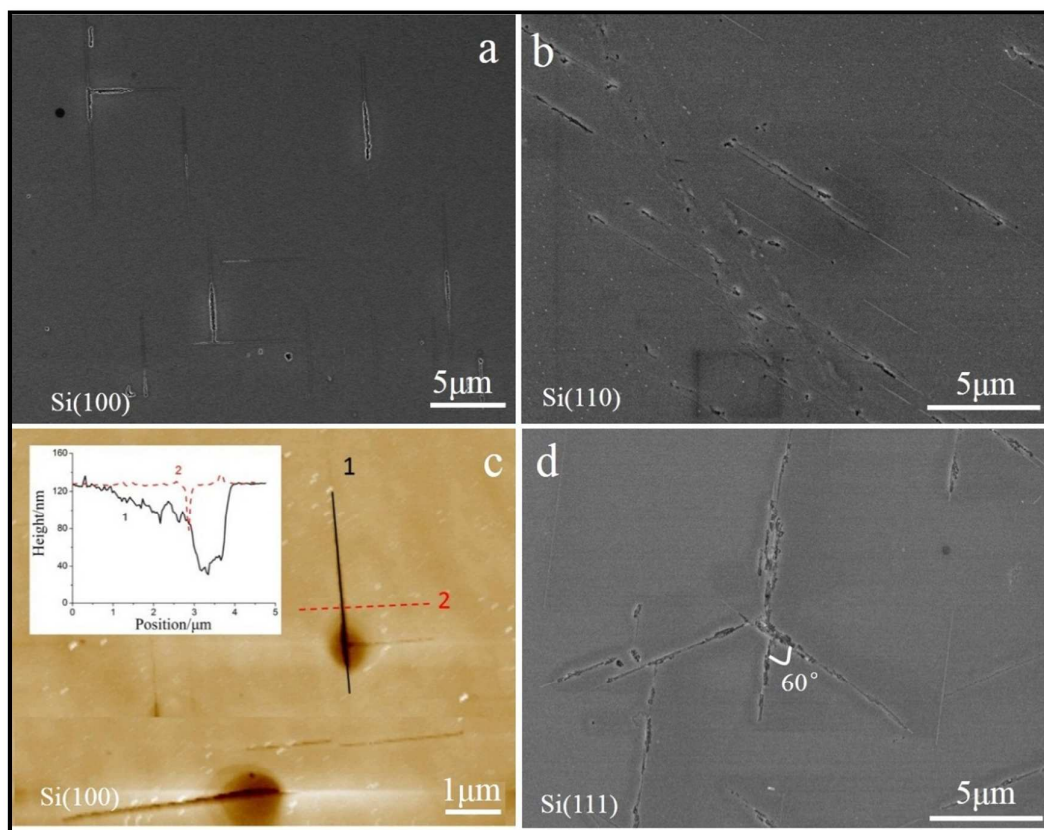


Fig. 6 (a–b, d) SEM micrographs of cracks on Si(110), (100), and (111) substrates, respectively. (c) AFM image of cracks on Si(100) substrate; the crack depth and width are approximately tens of nanometers and 100 nm, respectively.

To verify our hypothesis, we removed the B_2O_3 source, placed only Si substrate into the tube, and kept the other experimental conditions the same. Orientation-controlled cracks were obtained. Cracks on the Si(100) substrate are mutually orthogonal and are limited in two directions. For the Si(110) substrate, cracks form in one crystallographic direction only, whereas on the Si(111) substrate, cracks form in three directions, each at an angle of 60° to each other, as shown in Fig. 6. In a plasma condition, the Si<110> crystal orientation forms defects more easily. Figure 7a shows a schematic of the growth mechanism. i) B and N atom deposition on the substrate forms a BN film. Simultaneously, high-energy N or H atom or ion bombardment of the Si surface leads to the formation of defects along Si<110>. ii) N reacts with B in the defects to form BN and also tends to diffuse into the substrate and form an endotaxial Si_3N_4 nanostructure. iii) Endotaxial Si_3N_4 serves as a template for BN nanodot growth. iv) BN nanodots self-assemble into NWs. Figure 7b shows the density functional theory used to calculate a B–N–Si phase diagram³⁵. The calculated formation energies of BN, Si_3N_4 , and SiB_3 are -1.472 eV, -1.312 eV, and -0.041 eV,

respectively. The negative formation energy for BN and Si_3N_4 indicates that these phases are energetically favorable to form. A tie line exists between Si_3N_4 and BN, which means that the Si_3N_4 -BN system appears to be stable at room temperature. In short, endotaxial Si_3N_4 serves as a template for BNNW growth, which can be defined as self-templating growth.

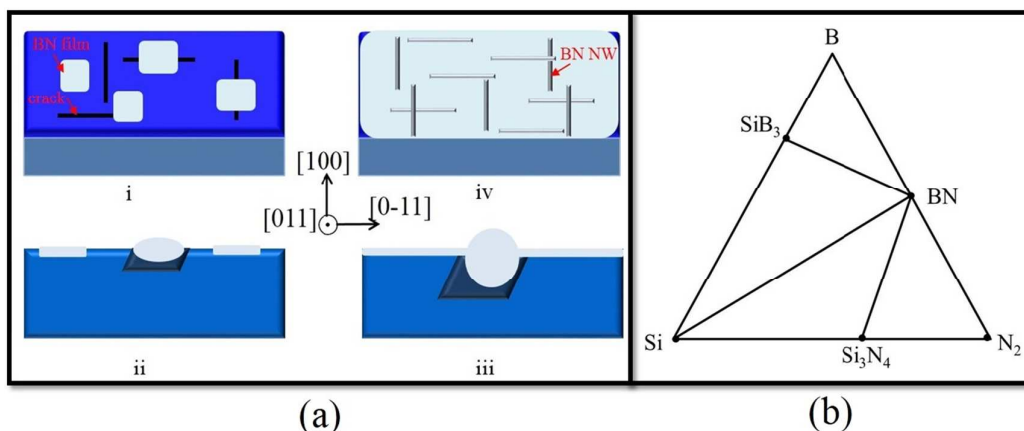


Fig. 7 (a) Schematic of NW growth: i) B and N atom deposition on substrate to form a BN film. Simultaneously, high energy N or H atom or ion bombardment of the Si surface forms defects along $\text{Si}\langle 110 \rangle$; ii) N reacts with B in the defects to form BN and tends to diffuse into the substrate to form an endotaxial Si_3N_4 nanostructure; iii) endotaxial Si_3N_4 serves as a template for BN nanodot growth; iv) BN nanodots self-assemble into NWs. (b) Calculated B–N–Si phase diagram.

We also measured the vertical electrical properties of the NW. Figure 8 shows a schematic of the measurement setup in C-AFM. Detailed data are provided in Fig. S3. By combining Fig. S3a and b, we see that current through the NW is larger than through other areas. The BN- Si_3N_4 -Si heterostructure may have a lower impedance than the BN-Si heterostructure because of the additional endotaxial Si_3N_4 structure and may lead to current through the NWs that is larger than that in the other areas. If the BN- Si_3N_4 -Si and BN-Si heterostructures present a different electrical performance, this may provide a possibility for fabricating novel nanoscale devices by the resistance effect. However, multiple challenges remain in this system, such as circumventing the reason for two different interfacial orientations and improving control of the endotaxial Si_3N_4 density and the BN crystallinity. The ability to tailor control of the density and position of the NW will improve developments to real-life applications of such nanodevices.

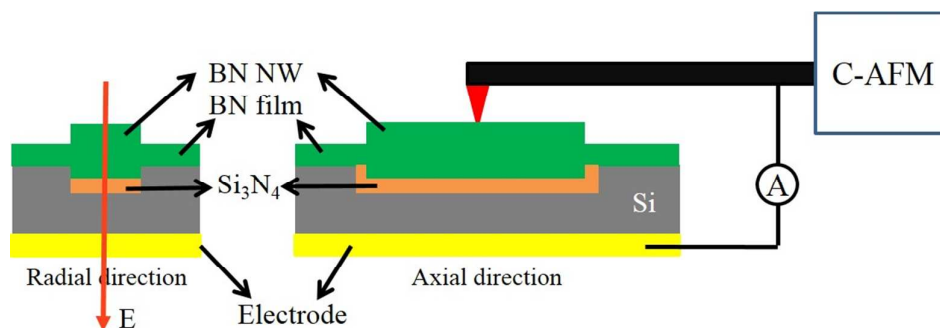


Fig. 8 Schematic of measurement set-up in C-AFM

Conclusions

In summary, we have reported a simple, environmentally friendly, economical technology to synthesize monolithic BNNWs by using only self-templating endotaxial NWs in the absence of any catalyst. The NW length reaches tens of microns with their orientation being fully controlled as a function of crystal orientation of the silicon substrate. The NW orientation is always along Si $\langle 110 \rangle$. It is proposed that BNNW growth originates from the template effect of endotaxial Si_3N_4 NWs. This self-templating synthesis for monolithic NWs could be extended to similar semiconductor materials, especially for elements that react with the substrate to form endotaxial NWs with a more favorable energy fit for the formed compound. Therefore, this work provides a means to synthesize monolithic NWs and a potential application of endotaxial NWs to produce single high-quality compound NWs for low-cost novel functional nanodevices.

Acknowledgments

The work was supported financially by the National Natural Science Foundation of China (NSFC) (Grant Nos 51472010 and 11274029), the Beijing Natural Science Foundation (2132014), the Jing-Hua Talents Project of Beijing University of Technology (No. 2014-JH-L07), the Foundation on the Creative Research Team Construction Promotion Project of the Beijing Municipal Institution (No. IDHT20140506), and the Importation and Development of High-Caliber Talents Project of the Beijing Municipal Institutions (No. CIT&TCD201204037).

References

1. X. Duan, Y. Huang, R. Agarwal and C. M. Lieber, *Nature*, 2003, **421**, 241-245.
2. C. M. Lieber and Z. L. Wang, *Mrs Bulletin*, 2007, **32**, 99-108.

3. A. I. Hochbaum and P. Yang, *Chemical reviews*, 2009, **110**, 527-546.
4. X. Duan and C. M. Lieber, *Advanced Materials*, 2000, **12**, 298-302.
5. M. J. Bierman, Y. A. Lau, A. V. Kvit, A. L. Schmitt and S. Jin, *Science*, 2008, **320**, 1060-1063.
6. H. Zeng, C. Zhi, Z. Zhang, X. Wei, X. Wang, W. Guo, Y. Bando and D. Golberg, *Nano letters*, 2010, **10**, 5049-5055.
7. A. Pakdel, C. Zhi, Y. Bando and D. Golberg, *Materials Today*, 2012, **15**, 256-265.
8. D. Golberg, Y. Bando, Y. Huang, T. Terao, M. Mitome, C. Tang and C. Zhi, *Acs Nano*, 2010, **4**, 2979-2993.
9. K. H. Lee, H. J. Shin, J. Lee, I. Y. Lee, G. H. Kim, J. Y. Choi and S. W. Kim, *Nano letters*, 2012, **12**, 714-718.
10. P. Ahmad, M. U. Khandaker, Z. R. Khan and Y. M. Amin, *Ceramics International*, 2014, **40**, 14727-14732.
11. Y. Cui and C. M. Lieber, *Science*, 2001, **291**, 851-853.
12. P. A. Smith, C. D. Nordquist, T. N. Jackson, T. S. Mayer, B. R. Martin, J. Mbindyo and T. E. Mallouk, *Applied Physics Letters*, 2000, **77**, 1399-1401.
13. R. F. Pease and S. Y. Chou, *Proceedings of the IEEE*, 2008, **96**, 248-270.
14. R. H. French and H. V. Tran, *Annual Review of Materials Research*, 2009, **39**, 93-126.
15. P. Hashemi, L. Gomez and J. L. Hoyt, *Electron Device Letters, IEEE*, 2009, **30**, 401-403.
16. R. G. Hobbs, N. Petkov and J. D. Holmes, *Chemistry of Materials*, 2012, **24**, 1975-1991.
17. J. C. Mahato, D. Das, R. R. Juluri, R. Batabyal, A. Roy, P. V. Satyam and B. N. Dev, *Applied Physics Letters*, 2012, **100**, 263117.
18. J. J. Zhang, G. Katsaros, F. Montalenti, D. Scopece, R. O. Rezaev, C. Mickel, B. Rellinghaus, L. Miglio, S. De Franceschi, A. Rastelli and O. G. Schmidt, *Phys Rev Lett*, 2012, **109**, 085502.
19. Z. Zhang, L. M. Wong, H. X. Wang, Z. P. Wei, W. Zhou, S. J. Wang and T. Wu, *Advanced Functional Materials*, 2010, **20**, 2511-2518.
20. S. Li, X. Huang, Q. Liu, X. Cao, F. Huo, H. Zhang and C. L. Gan, *Nano letters*, 2012, **12**, 5565-5570.
21. Y. Shen, S. Turner, P. Yang, G. Van Tendeloo, O. I. Lebedev and T. Wu, *Nano letters*, 2014, **14**, 4342-4351.
22. J. Nogami, B. Z. Liu, M. V. Katkov, C. Ohbuchi and N. O. Birge, *Physical Review B*, 2001, **63**, 3305.
23. P. A. Bennett, Z. He, D. J. Smith and F. M. Ross, *Thin Solid Films*, 2011, **519**, 8434-8440.
24. G. Kellermann, L. A. Montoro, L. J. Giovanetti, P. C. dos Santos Claro, L. Zhang, A. J. Ramirez, F. G. Requejo and A. F. Craievich, *Physical chemistry chemical physics : PCCP*, 2015, **17**, 4945-4951.
25. R. R. Juluri, A. Rath, A. Ghosh and P. V. Satyam, *The Journal of Physical Chemistry C*, 2013, **117**, 13247-13251.
26. Z. He, D. J. Smith and P. Bennett, *Physical review letters*, 2004, **93**, 256102.
27. R. W. Fathauer, J. M. Iannelli, C. W. Nieh and S. Hashimoto, *Applied Physics Letters*, 1990, **57**, 1419-1421.
28. T. George and R. W. Fathauer, *Applied Physics Letters*, 1991, **59**, 3249.
29. D. Sakellari, N. Frangis and E. Polychroniadis, *Physica E: Low-dimensional Systems and Nanostructures*, 2010, **42**, 1777-1780.
30. Y. Mo, J. Kleiner, M. Webb and M. Lagally, *Physical review letters*, 1991, **66**, 1998.
31. C. J. Wu and E. A. Carter, *Physical Review B*, 1992, **46**, 4651.
32. Y.-W. Mo, J. Kleiner, M. Webb and M. Lagally, *Surface science*, 1992, **268**, 275-295.
33. M. Tang, L. Colombo, J. Zhu and T. D. De La Rubia, *Physical Review B*, 1997, **55**, 14279.

34. Z. Zhang, L. M. Wong, H. G. Ong, X. J. Wang, J. L. Wang, S. J. Wang, H. Chen and T. Wu, *Nano letters*, 2008, **8**, 3205-3210.

35. Materials Project Home Page. <https://www.materialsproject.org>, Database version 0.5.1